Optical Materials 32 (2010) 1560–1567

Contents lists available at ScienceDirect

Optical Materials

journal homepage: www.elsevier.com/locate/optmat

EPR and vibrational studies of some tungstates and molybdates single crystals

H. Fuks [a], S.M. Kaczmarek [a,*], G. Leniec [a], L. Macalik [b], B. Macalik [b], J. Hanuza [b]

[a] Institute of Physics, Szczecin University of Technology, 17 Al. Piastów, 70-310 Szczecin, Poland
[b] Institute of Low Temperature and Structure Research, PAS, P. Nr 1414, 50-950 Wrocław 2, Poland

ARTICLE INFO

Article history:
Received 15 June 2010
Accepted 18 June 2010
Available online 14 July 2010

Keywords:
Double molybdates and tungstates
Raman spectroscopy
EPR
Dysprosium
Cerium
Gadolinium

ABSTRACT

$CsDy(MoO_4)_2$, $KY(MoO_4)_2$, $KCe(WO_4)_2$, $KDy(WO_4)_2$, $KGd(WO_4)_2$, $KLa_{0.25}Pr_{0.75}(MoO_4)_2$, $KLa_{0.995}Pr_{0.005}(MoO_4)_2$, $KLa_{0.25}Pr_{0.75}(WO_4)_2$ double molybdates and tungstates single crystals have been investigated using the Raman and EPR techniques.

1. Introduction

The studied materials belong to the large family of the rare earth (RE) tungstates and molybdates that can be divided into several structural types. Some of them consists the isolated $Mo(W)O_4$ tetrahedra and in the others penta- and hexa-coordinated polyhedra appear [1]. There is still a strong interest in the double molybdates and tungstates of alkali metals and rare earth elements of the $M^IM^{III}(MeO_4)_2$ stoichiometry (where M^I = K, Na, Li, M^{III} = Ln,Y, Me = W, Mo) [2–4]). The possibility of high doping of these crystals with different transition and rare earth elements allows the production of active solid state lasers, including thin disk lasers, with effective generating properties [5–9] as well as for ultrashort pulse laser systems [10]. $KRE(WO_4)_2$ can develop also dielectric planar waveguide designs (PWLs) [11,12].

Among the investigated crystals: $KY(MoO_4)_2$ crystal could be used in practice to build ribbon and sheet miniature lasers generating visible and infrared radiation [13]. Pr^{3+}: $KY(MoO_4)_2$ crystal is a candidate to microchip laser medium in the visible region [14]. For Nd: $KLa(MoO_4)_2$ a diode pumped CW laser was reported [15]. Dy^{3+} in $KY(WO_4)_2$, e.g. has gained interest due to its emission features in the 3 μm wavelength region, related to the $^6H_{13/2}$–$^6H_{15/2}$ transition [16]. The structure of the investigated crystals was analyzed in papers [17–37], while some EPR results were presented in [38–42].

The aim of the present work is studying the optical and EPR properties of some double molybdate and tungstate single crystals, and to make effort in explanation of significant differences in both those systems resulting from different structure and high content of paramagnetic ions.

2. Experimental setup

Single crystals of the double potassium and caesium rare earth molybdates and tungstates were grown by the thermal method developed by Borisov and Klevstova [17] and Klevtsov et al. [18]. The cooling rate was 2 °C per hour and the obtained crystals were transparent and of good optical quality. The samples were checked for purity by the X-ray powder diffraction.

The EPR spectra were recorded using Bruker E 500 X-band spectrometer (~9.4 GHz) at temperatures between 3 and 300 K. The first derivative of the power absorption spectra has been recorded as a function of the applied magnetic field. Temperature dependence of the EPR spectra was registered using an Oxford Instruments ESP helium-flow cryostat in the 8–295 K temperature range.

The Raman spectra of $KCe(WO_4)_2$ and $KDy(WO_4)_2$ were obtained using a conventional arrangement with 90° scattering geometry. A double-beam monochromator (f = 1 m) model DFS 24 with a photon counting detection system (cooled GaAs (USA) photomultiplier) were used. The excitation source was the 488 nm line of ILA 120 argon ion laser. The infrared absorption spectra of $CsDy(MoO_4)_2$ were recorded with a FT-IR BioRad 575C Spectrometer. Raman spectra of the others crystals presented in this paper were measured using Bruker RFS 100/S Raman Spectrometer with the back scattering arrangement. The 1064 nm line of Nd:YAG laser was used as an excitation source. Signal detection

* Corresponding author.
E-mail address: skaczmarek@zut.edu.pl (S.M. Kaczmarek).

0925-3467/$ - see front matter © 2010 Elsevier B.V. All rights reserved.
doi:10.1016/j.optmat.2010.06.018

was performed with an InGaAs detector. The measurements were performed with the 2 cm^{-1} spectral resolution.

3. Crystal structure and Raman spectra

The $KY(MoO_4)_2$ [19,20], $CsDy(MoO_4)_2$ [25] molybdates crystallise in the orthorhombic structure of the scheelite-like type in which the Dy^{3+} or Y^{3+} ions occupy the C_2 sites. The latter crystal undergoes a subsequent of phase transitions of the Jahn–Teller type at low temperature [26]. $KLa(MoO_4)_2$ and $KPr(MoO_4)_2$ are isostructural and crystallise at room temperature in the monoclinic space group $P2/n = C_{2h}^4$, $Z = 8$, in which the La^{3+} and Pr^{3+} ions occupy the sites of the C_1 symmetry and molybdate units appear as isolated tetrahedra [18,21–24]. $KCe(WO_4)_2$ belongs to the scheelite family and crystallises in the monoclinic space group $P2_1/c = C_{2h}^5$ with $Z = 4$ [18]. In this structure the tungstate units appear in the form of isolated tetrahedra and Ce^{3+} ions occupy the sites of the C_1 symmetry. The $KY(WO_4)_2$, $KDy(WO_4)_2$ and $KGd(WO_4)_2$ tungstates crystallise in the monoclinic structure $C2/c = C_{2h}^6$ with $Z = 4$ [23,27]. In this structure the tungstate units built the WO_6 octahedra joined through the single and double oxygen bridges. The RE^{3+} ions occupy the sites of C_i and C_2 symmetry. The $KLa(WO_4)_2$ and $KPr(WO_4)_2$, tungstates crystallise in the monoclinic space group $C2/m = C_{2h}^3$ with $Z = 4$ [18]. Their unit cell contains the sites of the C_2, C_i and C_s symmetry that can be substituted by the RE^{3+} ions.

From the structure considerations of the studied molybdates and tungstates it follows that in all these materials the RE^{3+} ions appear in the low-symmetry oxygen environment. The majority of them, except $CsDy(MoO_4)_2$, does not change their structure in the range 7–300 K [17,18,20,28–37].

Fig. 1 presents the room temperature Raman spectra (RS) of the studied compounds. They show the clear multiplets of the stretching ν(Mo(W)-O) vibrations in the range 750–1000 cm^{-1} and the bending vibrations in the range 300–450 cm^{-1}. The molybdates and tungstates built from the isolated tetrahedra exhibit the energy gap between the 450 and 750 cm^{-1} (e.g. $KLa_{0.25}Pr_{0.75}(MoO_4)_2$ and $KLa_{0.25}Pr_{0.75}(WO_4)_2$). On the other hand, the RS spectra of the materials with the polymeric structure ($KY(MoO_4)_2$, $KGd(WO_4)_2$ and $KDy(WO_4)_2$) show the bands in the gap region where the stretching modes of the M^OM and $M^O{}_OM$ oxygen bonds are observed. In all spectra the bands appeared below 300 cm^{-1} correspond to the external modes connected with the translational motions of the cations and anions, as well as vibrations of the molybdate or tungstate polyhedra.

All bands observed in the above spectra correspond to the phonon properties of the studied materials.

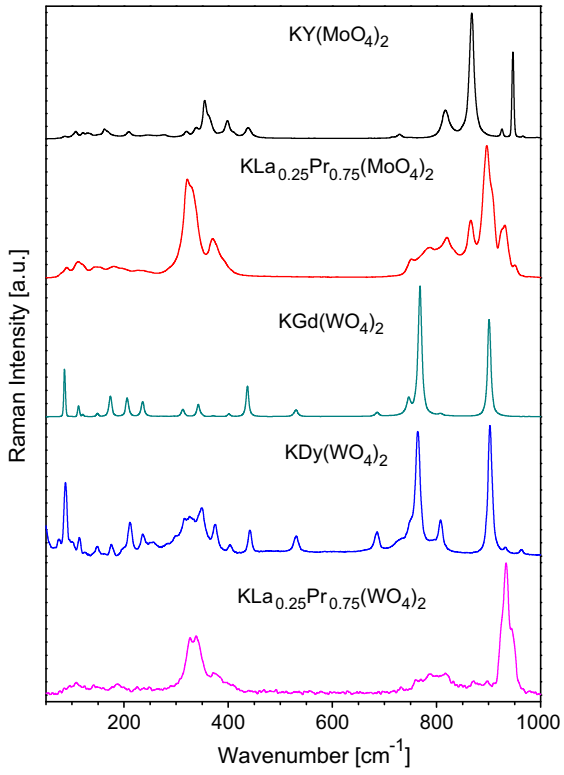

Fig. 1. Raman spectra of $KY(MoO_4)_2$, $KLa_{0.25}Pr_{0.75}(MoO_4)_2$, $KGd(WO_4)_2$, $KDy(WO_4)_2$ and $KLa_{0.25}Pr_{0.75}(WO_4)_2$ measured at room temperature.

4. EPR results

The shape of the EPR signal suggests that several spin systems can exist in the studied crystals forming a few non-equivalent magnetic centres. According to the crystal structure, in double tungstates and molybdates two kinds of paramagnetic centers could nominally exist: rare earth RE^{3+} ions with C_2 or lower point symmetry, located at distorted dodecahedra, and/or, reduced transition metal Me^{5+} ions located at tetrahedral or octahedral sites. The tungsten or molybdate center is expected to undergo two subsequent one-electron reductions from Me^{6+} to Me^{4+}. The intermediate Me^{5+} is paramagnetic and shows a typical $S = 1/2$ signal with g-factors usually below 2.0, which could be observable at temperatures as high as 100 K. RE^{3+} ions in the presented group of materials could not be treated only like an isolated paramagnetic centers but, due to significantly higher concentration, they could create a complex magnetic system (e.g. magnetic pairs or form a complex network).

A group of crystals has been investigated by using the EPR technique revealing the existence of the X-band resonance signal at temperatures below 60 K.

The EPR spectra of $CsDy(MoO_4)_2$ and $KDy(WO_4)_2$ crystals consist of a broad and asymmetric line (Fig. 2) attributed to the Dy^{3+} paramagnetic entities. An additional narrow signal visible at about 330 mT could be due to the Mo^{5+} or W^{5+} ions. Both of those lines emerge as reduced ions from the nominally non-magnetic 6+ state.

Due to high concentration of dysprosium, the hyperfine lines are suppressed in $CsDy(MoO_4)_2$, and, as a result, only one asymmetric broad line is observed. From our simulations it follows that the broad resonance line has mostly Gaussian line-shape. The best fit is obtained for combination of two line-shapes of the form: 65% G + 35% L. Domination of Gaussian shape points to significant dipole–dipole interactions in the Dy^{3+} magnetic system. Very similar shape of the EPR line we observed for $KDy(WO_4)_2$ crystal, although the effect of hyperfine interaction is additionally visible in this case. This agrees with the results obtained from the magnetization measurements reported in [43].

For the $CsDy(MoO_4)_2$ crystal, changes of the integral intensity I_{int} as a function of temperature follow the Curie–Weiss law, $I_{int} = C/(T-\theta)$, with negative Curie–Weiss temperature $\theta = -0.64$ K indicating on very weak antiferromagnetic interaction between Dy^{3+} ions. Signal from Mo^{5+} obeys C-W law with negative temperature parameter, $\theta = -1.07$ K, indicating antiferromagnetic interaction between molybdenum paramagnetic entities. Curie–Weiss law for Dy EPR line is satisfied only in a limited temperature region. The difference ΔI_{int} between the calculated value from the low-temperature Curie–Weiss law I_{int}^{CW} and observed in experiment $I_{int}^{obs.}$ grows as the temperature rises from 10 K and reaches a maximum at about 35 K. It could be analyzed in terms of the following equation [44]:

$$\Delta I_{int}(T) = \frac{\alpha}{T} \cdot \exp\left(-\frac{T_0}{T}\right) \quad (1)$$

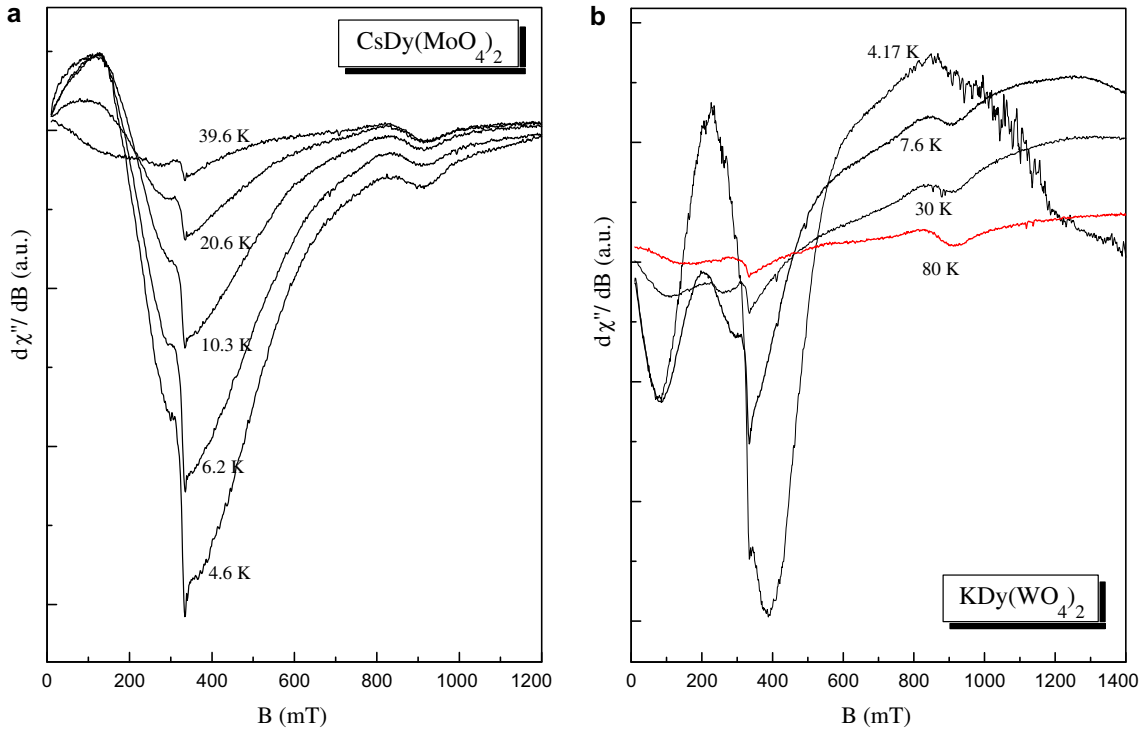

Fig. 2. The EPR spectra of $CsDy(MoO_4)_2$ (a) and $KDy(WO_4)_2$ (b) crystals measured at different temperatures (the signal at c.a. 900 mT is spurious).

where T_0 is the energy difference (expressed in K) between the ground state and the excited state. The equation suggests that the resonance spectrum reflects the existence of an excited state. The fitting of Eq. (1) to the experimental points shows that the excited state is about 35.4(2) K above the ground state. This is a typical value for Dy ions [45]. Between 10 K and 35 K the magnetic moment decrease with temperature increase which indicate that the first excited state is non-magnetic. From our fittings it follows that the EPR signal originates from the lowest ground state (Γ^6, Γ^7). Weak antiferromagnetic interaction observed at low temperatures changes to ferromagnetic one (θ = 15 K) at a temperature over 18 K. The character of linewidth changes (we observe its decrease with an increase of temperature below 18 K and strong increase over the temperature, up to 52 K) suggesting the influence of structural phase transition in that range. Phase transition of the Jahn–Teller type was observed previously in the crystal at T = 42 K by Geraschenko et al. [47] by the phonon and electronic absorption spectra investigation.

In the case of $KDy(WO_4)_2$ crystal, changes of the integral intensity I_{int} vs. temperature dependence follows the Curie–Weiss law, $I_{int} = C/(T-\theta)$, with positive θ = 2.96 K indicating possible ferromagnetic interactions between Dy^{3+} ions, whereas signal from W^{5+} obeys this law with the negative temperature parameter $\theta = -1.09$ K, indicating antiferromagnetic interaction between tungstate paramagnetic entities. In this case, however, a broad dysprosium line cannot be evaluated properly, due to a strong anisotropy of the line (Fig. 2b), because some components located in low magnetic fields are additionally observed. Curie–Weiss law is not fulfilled for almost all temperatures. However, the difference between I_{int}^{CW} and $I_{int}^{obs.}$ increases slightly up to about 6 K, passing a maximum. It may be an effect of structural phase transition. It was established in [48] that such kind of transition takes place in the crystal at T = 6.38 K.

We have performed simulations of the EPR spectra for both crystals using EPR–NMR program [49]. With this aim we separated two different lines attributed to Mo(W) and Dy ions. It is often assumed that Dy(III) could be described by an effective spin S_{eff} = 1/2 with anisotropic g values [38].

The following effective spin Hamiltonian, with only Zeeman term, for an effective spin S_{eff} = 1/2, was applied to EPR spectra of $CsDy(MoO_4)_2$:

$$H_S = \beta B \cdot g \cdot S \tag{2}$$

where all symbols have their usual meaning and an average g-factor is defined as $g = (g_{II} + 2 \cdot g_{\perp})/3$. Using spectra simulation, two different g values: $g_{\perp}$ = 2.59 and $g_{||}$ = 6.54 were obtained. This large anisotropy is possible because the Ising-like behavior is frequently exhibited by Dy(III)-containing compounds [38]. The g-factors indicate an axial symmetry of the paramagnetic centers.For the EPR spectra of $KDy(WO_4)_2$ crystal we applied the following spin Hamiltonian (for an effective spin S = 1/2 and nuclear I = 5/2):

$$H_S = \beta B \cdot g \cdot S + S \cdot A \cdot I + I \cdot P \cdot I \tag{3}$$

where all symbols have their usual meaning *and* A – hyperfine interaction matrix, P – the nuclear quadrupole coupling matrix [46]. Besides Zeeman term the hyperfine interaction and nuclear–quadrupol interaction terms have been taken into account. The values of spin Hamiltonian parameters are gathered in Table 1.

From magnetization measurements a possible magnetic structure of the ground state of the $KDy(WO_4)_2$ compound has been proposed. The magnetic structure represents the 3D system of Dy^{3+} ions ordered antiferromagnetically along the b-axis [43].

The EPR results for $KLa_{0.995}Pr_{0.005}(MoO_4)_2$ and $KLa_{0.25}Pr_{0.75}(MoO_4)_2$ crystals are shown in Fig. 3a and b. As the observed

Table 1
Spin-Hamiltonian parameters of Dy^{3+} ion in $KDy(WO_4)_2$ crystal derived from EPR–NMR program [49] (A_i and P_i values are in 10^{-4} cm^{-1}).

g_x	g_y	g_z	A_x	A_y	A_z	P_x	P_y	P_z
1.741	1.744	5.710	2600	−280	−690	190	−80	9

resonance signal revealed insignificant changes for two different Pr^{3+} concentrations, we could exclude the origin of the EPR signal from praseodymium ions. Non-magnetic state of Pr^{3+} shows typical behavior for non Kramers paramagnetic ions, where energy interval between ground $J = 0$ and excited $J = 1$ states is large. The observed EPR signal in this case may be attributed to reduced Mo^{5+} ions. Few resonance lines observed at fields below 250 mT could be assigned to small fraction of excited praseodymium magnetic centers.

For both praseodymium molybdates we have got a constant linewidth $\Delta B \sim 24$ mT and almost this same ferromagnetic interaction with Curie–Weiss parameter $\theta = 1.38$ K and $\theta = 2.05$ K for crystals with lower and higher Pr^{3+} contents, respectively. Similar EPR spectra we have been observed for $KLa_{0.25}Pr_{0.75}(WO_4)_2$ (Fig. 4a). The linewidth of W^{5+} ions in this case is $\Delta B \sim 21$ mT. Analysis of the I_{int}(T) function reveals a weak ferromagnetic interaction of prevalent ions in the praseodymium tungstate with $\theta = 0.47$ K.

Comparing spectra visible in Figs. 3 and 4a one can see that shape and intensity of the EPR signal, including position of the main resonance line (with evaluated $g_{eff} \approx 2.073$) are practically this same for all three praseodymium samples. This suggests that signal in $KLa_{0.25}Pr_{0.75}(WO_4)_2$ sample could originates not from W^{5+} ions but from Mo^{5+} impurities.

Thus, the EPR results for both praseodymium: molybdate and tungstate suggests that the transition metal ions are well isolated in these type of structures, showing only weak magnetic interaction.

Among presented group of crystals the most undoubtful spectra of RE^{3+} ions have been observed for the $KCe(WO_4)_2$ sample, where Ce^{3+} ions produce no hyperfine interactions and EPR spectra consist of a narrow intense line (Fig. 4b). Due to high intensity of Ce^{3+} signal, the resonance from W^{5+} ions is not observed in this case. The Curie–Weiss temperature, resulting from simulation of the total intensity, I_{int}, to Curie–Weiss law, was found to be about $\theta = -0.82$ K, suggesting slight antiferromagnetic interaction between Ce^{3+} ions. Detailed analysis of the I_{int}(T) dependence revealed some deviations from C–W model. It is most clearly observed in Fig. 5a which shows the $I_{int}{}^{*}T$ product as a function of temperature. The points in Fig. 5a follow with different slopes and, maximum of $I_{int}{}^{*}T$ dependence is observed at about 15 K. Changes of the slopes means that antiferromagnetic interaction of cerium ions dominates at low temperatures, below 15 K, while above 15 K ferromagnetic interaction prevails. Fittings of the I_{int} dependence vs. T using Bleaney–Bowers relation, usually applied for dimmers, gave an interaction parameter, J/k, of the order of 33 K, confirming ferromagnetic kind of interactions within 45% of all paramagnetic entities.

Nontrivial behavior of the magnetic Ce^{3+} ions is the result of their high concentration in an analyzed crystal. If cerium ions create a complex magnetic system (e.g. magnetic pairs), the existence of the excited ferromagnetic state is possible in high temperatures, whereas, as temperature decreases, the magnetic system undergoes transition to the energetically preferable antiparallel orientation.

Complex nature of Ce^{3+} magnetic system seems to be confirmed by observation of the peak to peak linewidth vs. temperature dependence. Fig. 5b shows typical one phonon behavior at lower temperatures, whereas width of the line significantly increases at temperatures above 40 K. Indeed in Fig. 5 the behaviour is 1 phonon at the lower temperatures and Raman + Orbach effect at the higher temperatures. Exponential change of the ΔB could be connected with the spin–lattice relaxation processes involving excited states of Ce^{3+} ions. At temperatures above 20 K the influence of the excited states could be expressed by the Orbach formula:

$$\Delta B = \Delta B_0 + A\, e^{-W/kT} \tag{4}$$

where: ΔB_0 – residual linewidth, A – experimental parameter, W – energy difference between the ground and the first excited state, k – the Boltzmann constant. The results of the simulation by using Orbach formula are shown as a solid line in Fig. 5b. Calculated parameters are: $\Delta B_0 = 120$ mT, $A = 14.200$ mT, $W/k = 333$ K.

Oriented $KCe(WO_4)_2$ single crystal has been investigated by rotating it around the c-crystallographic axis. As it is seen in Fig. 6a several components of the cerium resonance signal can be distinguished. The whole dependence of four resonance transitions

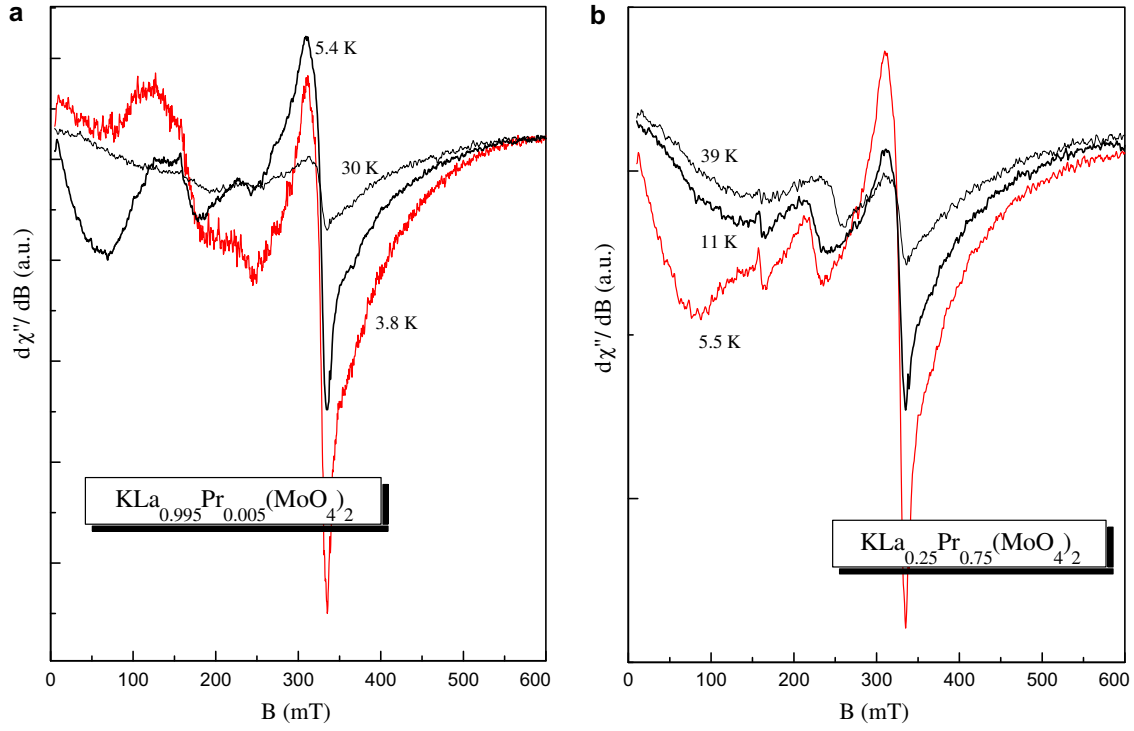

Fig. 3. The EPR spectra of $KLa_{0.995}Pr_{0.005}(MoO_4)_2$ (a) and $KLa_{0.25}Pr_{0.75}(MoO_4)_2$ (b) crystals registered at different temperatures.

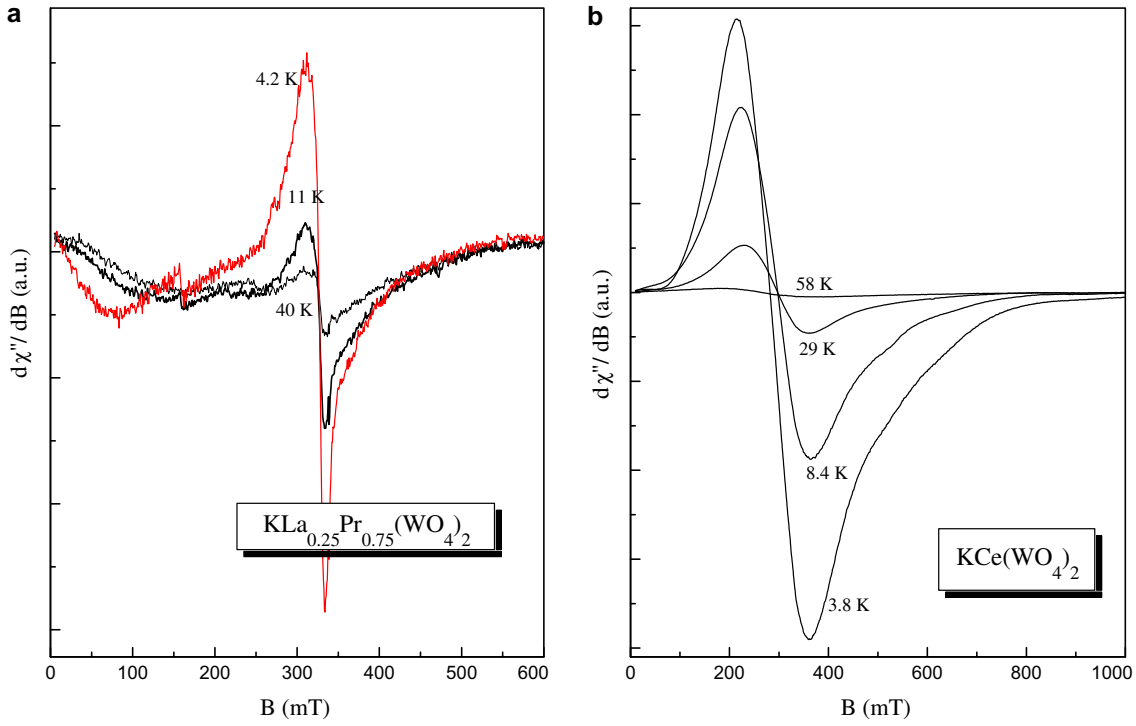

Fig. 4. The EPR spectra of $KLa_{0.25}Pr_{0.75}(WO_4)_2$ crystal (a) and $KCe(WO_4)_2$ crystal (b) measured at different temperatures.

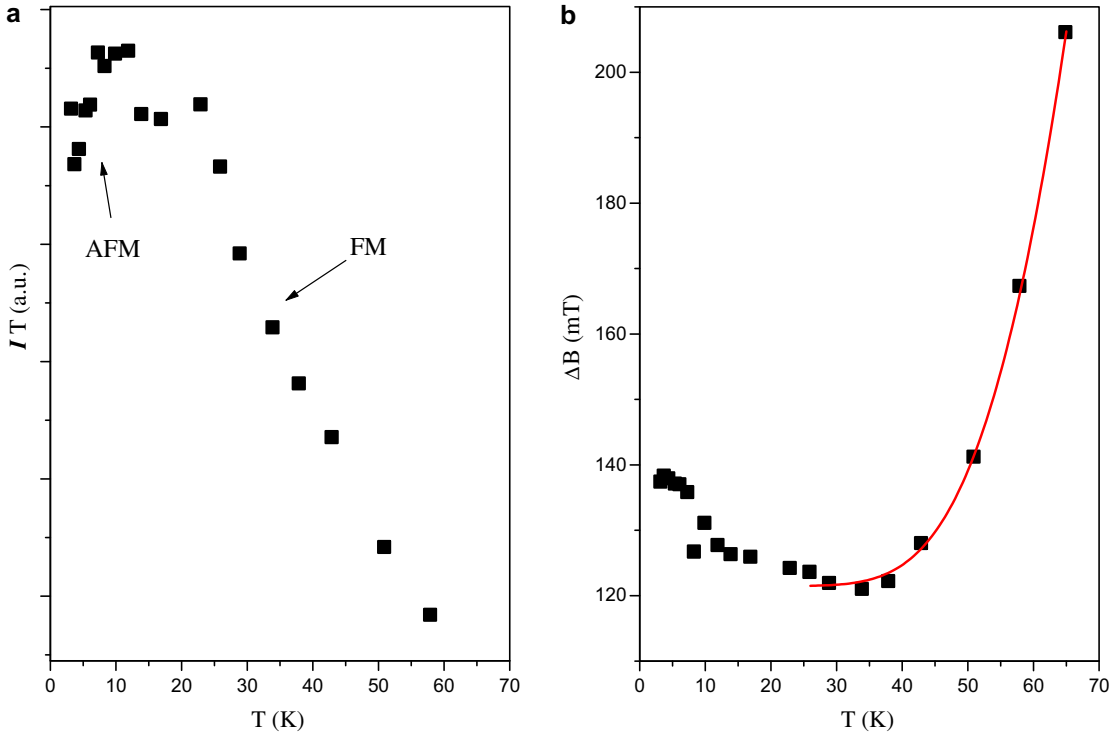

Fig. 5. The dependence of the $I_{int}^{*}T$ product on temperature (a) and the relation of peak to peak linewidth vs. temperature (b) for $KCe(WO_4)_2$ crystal.

as a function of rotation angle is shown in Fig. 6b. As one can see the components of the EPR signal change in the range c.a. g_{eff} = 2.248–2.879 at angle 0°, whereas at angle 90° the splitting is higher with g_{eff} = 1.102–4.299. The pattern is not resolved in this case, mainly due to complex nature of the Ce^{3+} magnetic centers, but as the roadmap is repeatable with 180° step we can conclude that the Ce^{3+} magnetic centers have C_2 or lower (C_1) local symmetry.

The EPR spectra of $KGd(WO_4)_2$ sample revealed a broad asymmetric line due to Gd^{3+} ions (Fig. 7a) placed at different

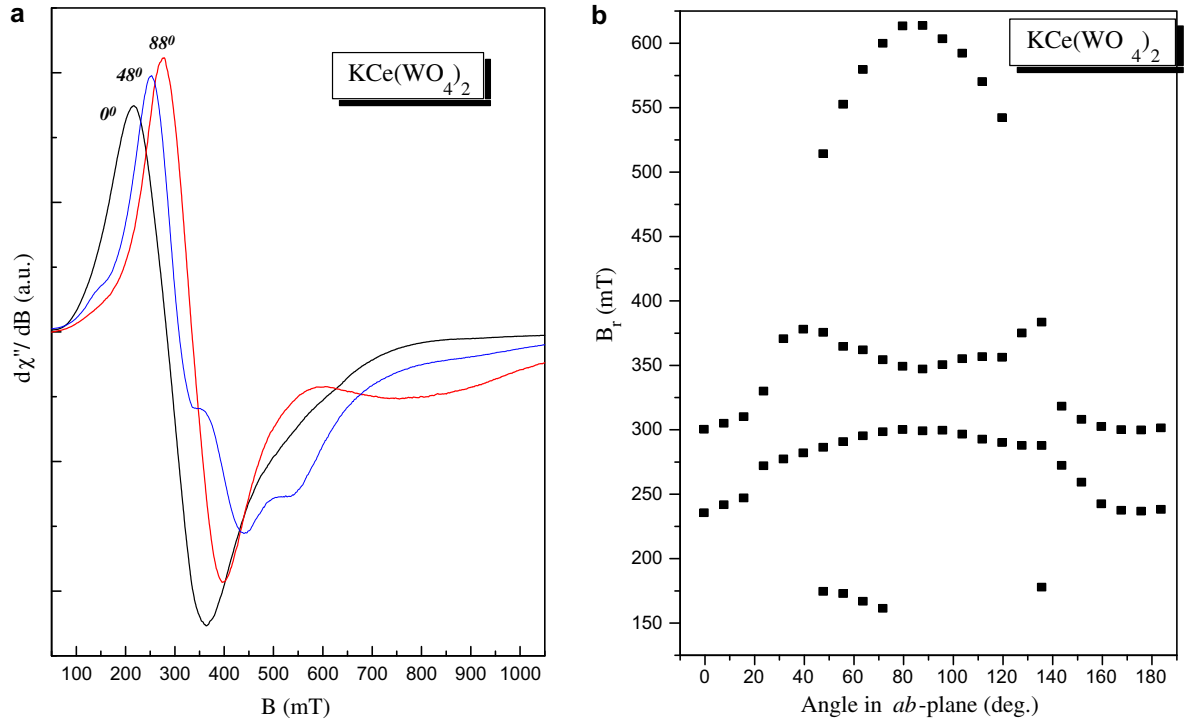

Fig. 6. The EPR spectra of $KCe(WO_4)_2$ crystal measured for different angles at 7 K (a) and the resonance field of all components of the EPR signal as a function of rotation angle (b).

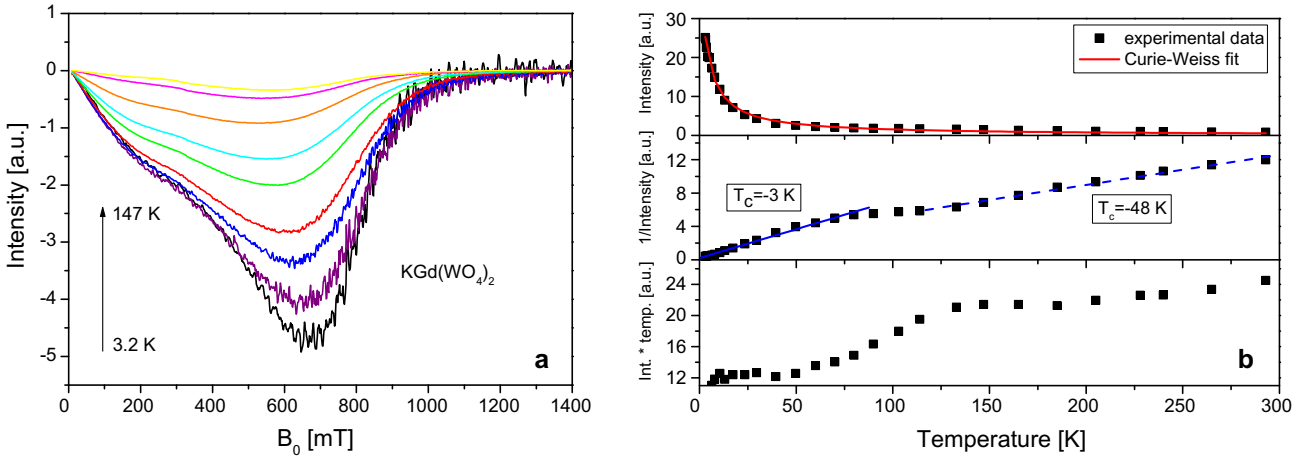

Fig. 7. (a) The EPR spectra of $KGd(WO_4)_2$ crystal measured at different temperatures, and (b) temperature dependence of the integral intensity, reciprocal of the intensity and the product of the intensity and temperature for $KGd(WO_4)_2$ single crystal.

symmetry sites. The shape of the resonance line, consisting of at least two component lines, seems to be a combination of Gaussian and Lorentzian like functions; similar situation we observed for Dy^{3+} ions, what indicates on the existence of dipole–dipole interaction besides the exchange interaction between the gadolinium ions.

The gadolinium line is visible in a wide temperature range and reveals Curie–Weiss behavior with relative high value: $\theta = -3$ K in low temperature range (below 75 K) and, $\theta = -48$ K in higher temperatures, reflecting antiferromagnetic interaction between Gd^{3+} ions (Fig. 7b upper and middle panels). Magnetic moment increases with temperature increase (Fig. 7b, lower panel), *g*-factor shows anomaly at low temperatures suggesting the presence of some kind of internal magnetic field, assigned e.g. to 1D chains (Fig. 8, middle panel). Other parameters of the spin-Hamiltonian ($S = 7/2$, Eq. (5)) are presented in Fig. 8

$$H_S = \beta BgS + \sum_m \sum_n B_n^m O_n^m \tag{5}$$

First term in Eq. (5) is the Zeeman term, whereas the second one represents the sum of crystal field parameters (standard Stevens coefficients and operators).

As one can see the local symmetry of Gd^{3+} ions is at least monoclinic. Although general conclusions on the local symmetry of the Gd^{3+} ions in $KY(WO_4)_2$ lattice are the same, differences between parameters of the spin-Hamiltonian derived for diluted

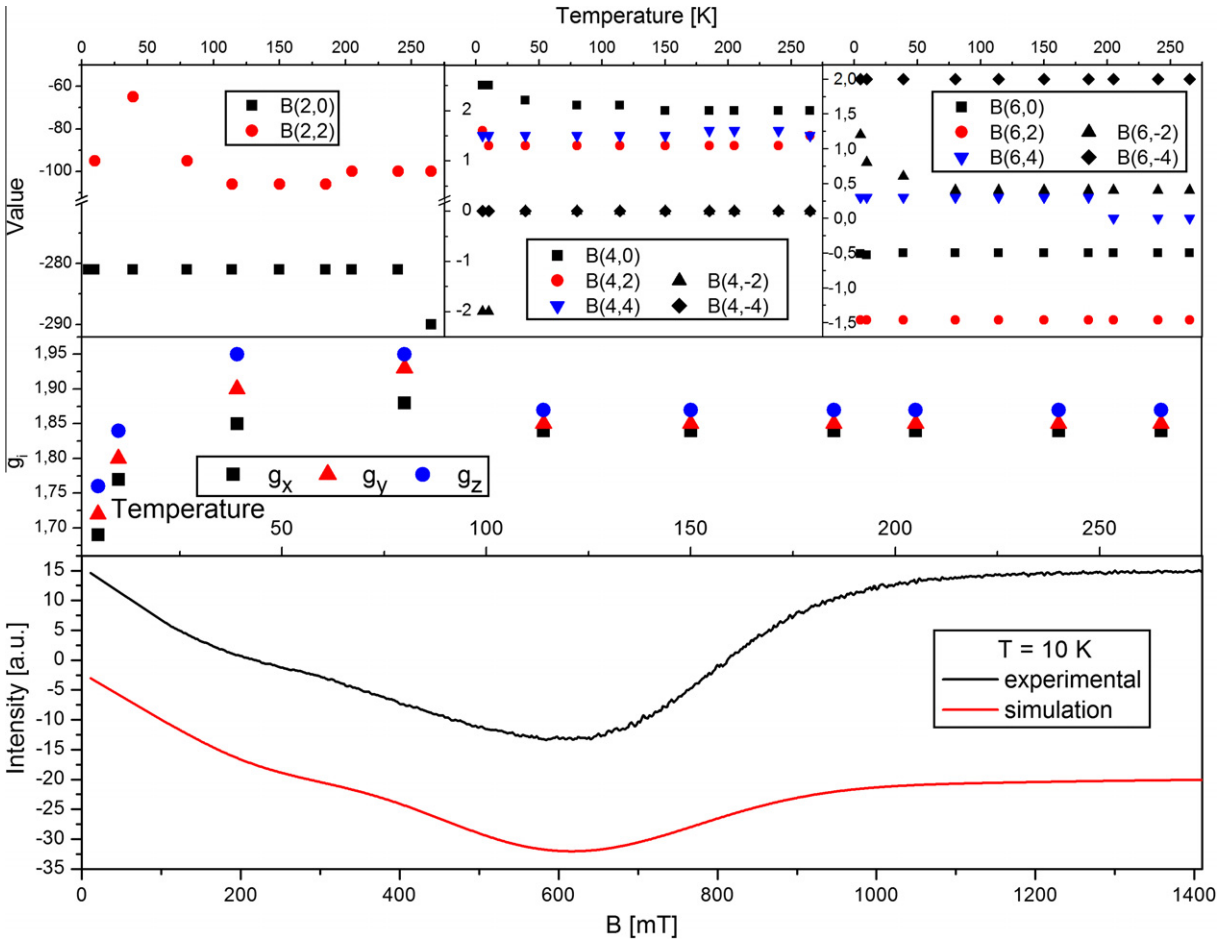

Fig. 8. Spin-Hamiltonian parameters of the $KGd(WO_4)_2$ compound: Stevens parameters (upper panel), *g*-factors (middle panel) and experimental vs. simulation shape of the EPR spectrum.

$KY(WO_4)_2$:Gd^{3+} and concentrated $KGd(WO_4)_2$ crystal occur, as reported in [41]. Low values of *g* suggests the presence of additional types of magnetic interactions in concentrated ($KGd(WO_4)_2$) compound with respect to diluted one. The same concerns to Stevens parameters.

5. Conclusions

EPR study of rare-earth double molybdates and tungstates revealed the presence of magnetic centres of two kinds: RE^{3+} and well isolated Mo^{5+} or W^{5+}, where pentavalent transition ions are created from reduced 6+ ions. The RE^{3+} ions revealed significant dipole–dipole interactions which lead to creation of developed magnetic system having weak ferromagnetic nature. These results are consistent with previous reports concerning double molybdates and tungstates [40,42], indicating that RE^{3+} ions may form low dimension chains, usually along *a*-crystal axis.

If crystal is doped by magnetically silent RE^{3+} ions the pentavalent transition metal ions become more visible, usually as isolated paramagnetic entities, (see Figs. 3 and 4a) and they could form complex magnetic systems, as was observed by us in the case of $KY(MoO_4)_2$ crystal (the results are not presented here).

The strength of magnetic interactions is relatively high for Gd^{3+} ions, because gadolinium ion is a specific RE^{3+} ion with orbital moment equal to zero. As the analyzed crystals are heavily doped with RE^{3+} ions, the hyperfine structure is invisible, excluding $KDy(WO_4)_2$ crystal.

References

[1] J. Hanuza, K. Hermanowicz, L. Macalik, M. Mączka, P.E. Tomaszewski, Wiadomości Chemiczne, Poland, Wrocław (2008) 337–362.
[2] G. Blasse, Struct. Bonding 42 (1980) 1.
[3] A.A. Kaminskii, N.R. Agamalyan, L.P. Kozeeva, V.F. Nesterenko, A.A. Pavlyuk, Phys. Status Solidi A 75 (1983) K1.
[4] A.A. Kaminskii, Phys. Status Solidi A 148 (1995) 9.
[5] X. Mateos, V. Petrov, M. Aguiló, R. Solé, Jna. Gavaldá, J. Massons, F. Díaz, U. Griebner, IEEE J. Quantum Electron. 40 (2004) 1056.
[6] O. Silvestre, M.C. Pujol, M. Rico, F. Güell, M. Aguiló, F. Díaz, Appl. Phys. B 87 (2007) 707.
[7] X. Mateos, R. Solé, Jna. Gavaldá, M. Aguiló, J. Massons, F. Díaz, Opt. Mater. 28 (2006) 423.
[8] C. Zaldo, M. Rico, C. Cascales, M.C. Pujol, J. Massons, M. Aguiló, F. Díaz, P. Porcher, J. Phys.: Condens. Matter 12 (2000) 1.
[9] S. Rivier, X. Mateos, O. Silvestre, V. Petrov, U. Griebner, M.C. Pujol, M. Aguiló, F. Díaz, S. Vernay, D. Rytz, Opt. Lett. 33 (2008) 735.
[10] T.T. Basiev, A.A. Sobol, P.G. Zwerev, V.V. Osiko, R.C. Powell, Appl. Opt. 38 (1999) 594.
[11] Y.E. Romanyuk, C.N. Borca, M. Pollnau, S. Rivier, V. Petrov, U. Griebner, Opt. Lett. 31 (2006) 53.
[12] S. Rivier, X. Mateos, V. Petrov, U. Griebner, Y.E. Romanyuk, C.N. Borca, F. Gardillou, M. Pollnau. Opt. Exp. 15 (2007) 5885.
[13] A.A. Kaminskii, S.N. Bagayev, Quantum Electron. 24 (1994) 1029–1030.
[14] W. Guo, Y. Lin, X. Gong, Y. Chen, Z. Luo, Y. Chuang, J. Phys. Chem. Sol. 69 (2008) 8.
[15] Y. Ye, X. Long, W. Lin, J. Li, G. Wang, Opt. Mater. 30 (2007) 231.
[16] M. Malinowski, P. Myziak, R. Piramidowicz, I. Pracka, T. Łukasiewicz, B. Surma, S. Kaczmarek, K. Kopczyński, Z. Mierczyk, Acta Phys. Pol. A 90 (1996) 181.
[17] S.V. Borisov, R.F. Klevtsova, Kristallografiya 13 (1968) 517.
[18] P.V. Klevtsov, L.P. Kozeeva, L.Yu. Kharchenko, Kristallografiya 20 (1975) 1210.
[19] R.F. Klevtsova, S.W. Borisov, Dokl. Acad. Nauk SSSR 177 (1967) 1333.
[20] J. Hanuza, L. Labuda, J. Raman Spectr. 11 (1981) 231.
[21] B.M. Sokolovskyi, A.A. Evdokimov, V.K. Trunov, Zh. Neorgan. Khim. 22 (1977) 1499.

[22] P.V. Klevtsov, R.F. Klevtsova, Zh. Strukt. Khim. 18 (1977) 419.
[23] P.V. Klevtsov, L.P. Kozeeva, A.A. Pavlyuk, Kristallografiya 20 (1975) 1216.
[24] B.H. Wanklyn, F.R. Wondre, J. Cryst. Growth 43 (1978) 93.
[25] V.A. Vinokurov, P.V. Klevtsov, Kristallografiya 17 (1972) 127.
[26] V.I. Fomin, V.P. Gnezdilov, V.V. Eremenko, N.M. Nesterenko, Sov. Phys. Solid State 31 (1989) 871.
[27] L. Macalik, J. Hanuza, B. Macalik, W. Ryba-Romanowski, S. Gołąb, A. Pietraszko, J. Luminesc. 79 (1998) 9.
[28] P.V. Klevtsov, L.P. Kozeeva, A.A. Pavlyuk, Kristallografiya 20 (1975) 6.
[29] L.P. Solovyova, S.V. Borisov, Kristallografiya 14 (1969) 613.
[30] J. Hanuza, Acta Phys. Polon. A70 (1986) 585.
[31] J. Hanuza, L. Macalik, Spectrochim. Acta 43A (1987) 361.
[32] J. Hanuza, L. Macalik, K. Hermanowicz, J. Mol. Struct. 319 (1994) 17.
[33] L. Macalik, J. Mol. Struct. 404 (1994) 213.
[34] L. Macalik, J. Hanuza, J. Sokolnicki, J. Legendziewicz, Spectr. Acta 55A (1999) 251.
[35] L. Macalik, J. Hanuza, A.A. Kaminskii, J. Raman Spectr. 33 (2002) 92.
[36] S.S. Gerashenko, O. Miloslavskaya, Yu.N. Kharchenko, V.I. Kutko, N.M. Nesterenko, L. Macalik, K. Hermanowicz, M. Mączka, J. Hanuza, Mater. Sci. 20 (2002) 81.
[37] M. Mączka, J. Hanuza, J.-H. Ko, S. Kojima, Phys. Rev. B 68 (2003) 174101-1-8.
[38] M.T. Borowiec, V. Dyakonov, A. Prokhorov, H. Szymczak, Phys. Rev. B 62 (2000) 5834.
[39] M.T. Borowiec, V. Dyakonov, S. Piechota, A. Prokhorov, Phys. B 240 (1997) 21.
[40] M.T. Borowiec, V. Dyakonov, A. Jedrzejczak, V. Markovich, A. Pavlyuk, H. Szymczak, E. Zubov, M. Zaleski, Phys. Lett. A 243 (1998) 85.
[41] N.W. Chernyi, W.A. Nadolinnyi, Zawodska Laboratoria, Diagnost. Mater. 72 (2) (2006) 20.
[42] A.D. Prokhorov, M.T. Borowiec, V.P. Dyakonov, V.I. Kamenev, A.A. Prokhorov, P. Aleshkevych, T. Zayarnyuk, H. Szymczak, Phys. B 403 (2008) 3174.
[43] M.T. Borowiec, V. Dyakonov, I. Fita, A. Nabiałek, A. Pavlyuk, A. Szewczyk, H. Szymczak, M. Załęski, E. Zubov, J. Magnet. Mag. Mater. 195 (1999) 119–124.
[44] J. Yoshikawa, C. Urakawa, H. Ohta, T. Koide, T. Kawamoto, Y. Fujiwara, Y. Takeda, Phys. E 10 (2001) 395.
[45] G. Leniec, S.M. Kaczmarek, J. Typek, B. Kołodziej, P. Przybylski, B. Brzeziński, E. Grech, J. Non-Cryst. Sol. 355 (2009) 1355.
[46] J.A. Weil, J.R. Bolton, Electron Paramagnetic Resonance – Elementary Theory and Practical Applications, second ed., John Wiley & Sons, New Jersey, 2007.
[47] S.S. Geraschenko, O.V. Miloslavskaya, Yu.N. Kcharchenko, V.I. Kut'ko, N.M. Nesterenko, L. Macalik, K. Hermanowicz, J. Hanuza, J. Mol. Str. 563–564 (2001) 359.
[48] V.P. D'yakonov, V.I. Markovich, V.L. Kovarski, A.V. Markovich, Phys. Solid State 40 (1998) 691.
[49] M.J. Mombourquette, J.A. Weil, D.G. McGavin, EPR–NMR User's Manual, Department of Chemistry, University of Saskatchewan, Saskatoon, SK, Canada, 1999.